

Article

Anti-Condensation Temperature Control Strategy of the Concrete Radiant Roof

Bobo Zhang^{1,2,3,*}, Qin Sun^{1,2,3}, Lin Su^{1,2,3}, Kaijun Dong^{1,2,3,*}, Weimin Luo^{1,2,3}, Haifeng Guan^{1,2,3}, Zhenhua Shao^{1,2,3} and Wei Wu⁴

¹ Guangzhou Institute of Energy Conversion, Chinese Academy of Sciences, Guangzhou 510640, China; sunqinsq@hotmail.com (Q.S.); sulin87@163.com (L.S.); luowm@ms.giec.ac.cn (W.L.); guanhf@ms.giec.ac.cn (H.G.); shaozh@ms.giec.ac.cn (Z.S.)

² CAS Key Laboratory of Renewable Energy, Guangzhou 510640, China

³ Guangdong Provincial Key Laboratory of New and Renewable Energy Research and Development, Guangzhou 510640, China

⁴ School of Energy and Environment, City University of Hong Kong, Hong Kong, China; weiwu53@cityu.edu.hk

* Correspondence: zhangbb@ms.giec.ac.cn (B.Z.); dongkj@ms.giec.ac.cn (K.D.)

Abstract: Radiation cooling, as a new terminal mode that has been gradually emerging in recent years, has attracted more and more attention. However, the problem of condensation has become a vital bottleneck restricting the broad application of radiation-cooling technology. This paper used the numerical simulation method of Ansys Fluent to study the effect of different water supply parameters on the concrete radiant roof's heat transfer performance, temperature uniformity analysis, and anti-condensation temperature control strategy. The accuracy of the simulation model was verified by comparing the numerical simulation values and measured values of temperature monitoring points. In thermal performance research, the inlet temperature significantly impacted the cooling capacity and radiant surface temperature compared with the inlet flow velocity. In the uniformity study, the distance between the serpentine pipes area and the concrete edge was easily neglected, which was also an important factor affecting the distribution of temperature uniformity. Regarding anti-condensation and performance improvement research, first supplying water at low temperatures and then dynamically adjusting high-temperature water could effectively avoid condensation and improve the radiant roof's heat transfer performance. The research results could provide technical references for the practical application of radiation roof anti-condensation temperature control technology.

Keywords: radiation cooling; concrete radiant roof; serpentine pipe; anti-condensation; temperature control; computational fluid dynamics



Citation: Zhang, B.; Sun, Q.; Su, L.; Dong, K.; Luo, W.; Guan, H.; Shao, Z.; Wu, W. Anti-Condensation Temperature Control Strategy of the Concrete Radiant Roof. *Energies* **2023**, *16*, 4826. <https://doi.org/10.3390/en16124826>

Academic Editor: F. Pacheco Torgal

Received: 11 May 2023

Revised: 15 June 2023

Accepted: 19 June 2023

Published: 20 June 2023



Copyright: © 2023 by the authors. Licensee MDPI, Basel, Switzerland. This article is an open access article distributed under the terms and conditions of the Creative Commons Attribution (CC BY) license (<https://creativecommons.org/licenses/by/4.0/>).

1. Introduction

Radiation cooling, as a new terminal mode that has been gradually emerging in recent years, has advantages such as good thermal comfort, high energy efficiency, and peak power transfer, and has attracted more and more attention [1–3]. Radiation cooling directly exchanges heat with the surface of the human body through radiation so that the human body cannot feel the sensation of air blowing. Its thermal comfort is better than traditional convection-type air conditioning [4]. For some radiation applications with high thermal inertia, such as a concrete radiant cooling system, its structure can be used to play a certain role in energy storage. According to Olesen et al. [5], energy storage and the peak-filling of a radiant floor can save up to 50% of the energy consumption of cooling machines at peak times. With increasing living standards and awareness of low carbon and energy saving, people have higher and higher requirements for the comfort and energy saving of air conditioning. Concrete radiation cooling technology is an advanced technology that meets users' needs and is worth vigorously promoting.

However, there is also the problem of condensation at the radiation-cooling terminal mode. When the surface temperature of the radiant plate is lower than the dew point temperature of the surrounding air, condensation will occur in the area of low temperature. At the same time, there may be a risk of drops falling, making people uncomfortable [6]. Dew can damage the original decorative surface of the building and lead to mildew and sanitation problems [7,8]. Condensation has become a critical problem affecting the application of radiation cooling, especially in humid regions [9], and has become a vital bottleneck restricting the broad application of radiation-cooling technology.

There are numerous studies on solving the condensation problem for radiation-cooling panels. Radiant cooling panels are panels with controllable surface temperatures embedded in the ceiling, floor, or walls. The surface temperature can be determined by a specific water flow temperature in the embedded pipes hidden in the panel [10]. It is easy to imagine the effect of the water flow on condensation. Jin et al. [11] and Jin et al. [12] respectively studied the influence of water supply flow regulation and water supply temperature regulation on the dynamic temperature change in radiant roof surfaces. When the chilled water supply was closed or the water supply temperature rose, it could effectively prevent condensation on the surface of the radiant roof. However, in the case of high indoor humidity, this method quickly causes the problem of insufficient cooling capacity. Wongkee et al. [13] gave the limited cooling capacity of the studied radiant cold plate in tropical climates as 30 W/m^2 . In order to overcome the above difficulties, some latent heat processing systems (the parallel ventilation system [14], the additional jet and displacement ventilation air conditioning system [15], the desiccant dehumidification membrane [16], and vacuum membrane-based dehumidification [17]) were studied to work with the radiation cooling systems. The addition of the latent heat treatment system improved the cooling performance of the radiant plate but also increased the amount of equipment and energy consumption of the system. In addition, there were also some ways to treat the surface structure of the radiant panel to prevent condensation. Tang et al. [18] studied that the radius of droplets formed on the surface of the radiation plate with superhydrophobic surface treatment was less than $300 \mu\text{m}$, which was smaller than the human sensory threshold radius of droplets of $325 \mu\text{m}$. These results showed that superhydrophobic surfaces could significantly reduce condensation risks of radiant cooling ceiling systems. Ning et al. [19] proposed an infrared transparent cover to prevent condensation on the radiant cooling surface, which overcame the limitation of dewpoint temperature on the cooling ability of the radiant cooling surface to a certain extent. Kong et al. [20] provided a “drainage condensation” type radiation panel. The panel opened a dense microchannel on the surface of the radiant plate. It used capillary force and gravity to guide the condensation generated on the surface of the radiant plate to the edge to be collected. The above radiant panel surface treatment method had an outstanding advantage over the addition of other latent heat processing systems in that no additional energy consumption was required to achieve condensation prevention.

Although there were many ways to prevent condensation, no matter which method, it was impossible to ignore the influence of water supply parameters on the surface temperature of the radiant panel. The water supply was the cold source for radiant cold plate cooling. Its effect occurred before all anti-condensation controls. A reasonable water supply strategy could be combined with other anti-condensation methods to produce a superimposed condensation effect. However, few researchers have paid attention to this area of research. In some existing studies, research was limited to directly increasing the temperature of the water supply or turning off the water supply flow [11,12]. Therefore, it was necessary to study the influence of different combined water supply parameters on the radiant cold plate’s surface temperature and cooling capacity.

This work studies the anti-condensation effect of a radiant concrete roof under different combined water supply parameters. The novelty of this study was not only to prevent condensation but also to improve the cooling performance of the radiant roof. The computational fluent dynamics (CFD) simulation with Ansys Fluent was used to simulate the heat transfer of the radiant concrete roof, which was verified by the experimental data.

This study aimed to obtain an effective and high-performance anti-condensation control strategy based on water supply parameter adjustment so that the radiation roof could further improve its performance while the effects of condensation could be improved. The research results could provide technical references for applying the radiation roof anti-condensation control technology based on water supply parameter adjustment.

2. Simulation Methods

2.1. Physical Model

In this paper, a radiation roof of concrete was selected as the object of the simulation. As shown in Figure 1, the concrete radiant roof model consisted of two parts: a concrete structure and two serpentine pipes. In actual use, the radiation roof is installed on the ceiling of the room. Therefore, the radiant heat exchange surface refers to the bottom surface of the radiant roof. The specific dimensions of the concrete radiant roof model are shown in Figure 2. Two serpentine pipes were buried 40 mm from the radiant heat exchange surface, staggered and evenly arranged. When chilled water was injected into two serpentine pipes, the distance between adjacent pipes was 150 mm. The wall thickness of the serpentine pipes was so small in the global dimension that it could be ignored to simplify the calculation. Both serpentine pipes were 20 mm in diameter.

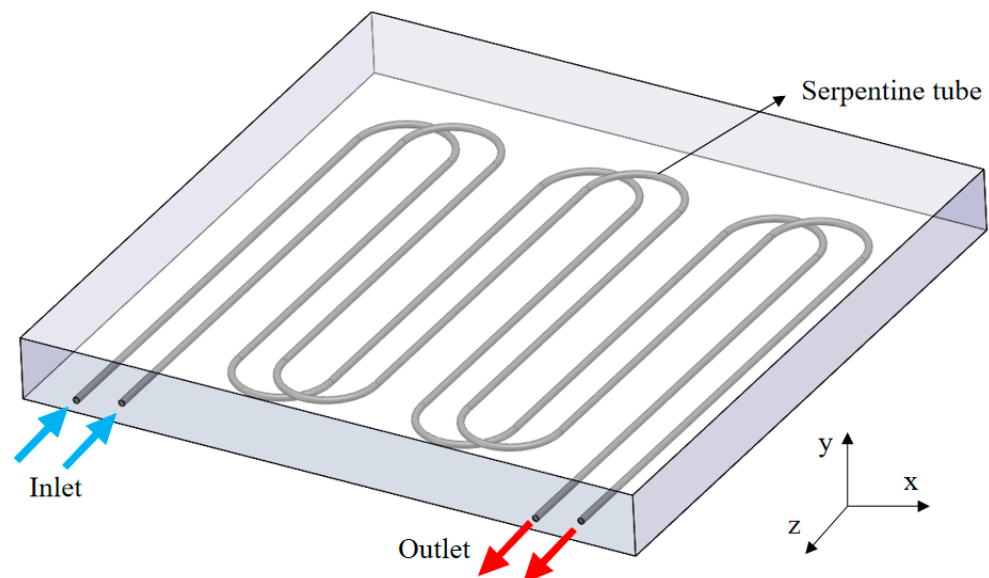


Figure 1. Three-dimensional structural diagram of the concrete radiant roof model.

2.2. Meshing

ICEM CFD 18.0 was used as the meshing software for the simulation, which could automatically generate tetrahedral meshes and Mitsubishi cylinder meshes describing boundaries for complex models. The mesh size of the area can be specified in the geometric model during meshing. For areas that have little influence on the calculation results, a larger mesh size can be set to reduce the amount of calculation for grid generation and improve the efficiency of numerical computation. For areas where the calculation results have an enormous impact, the mesh should be properly encrypted, and a smaller mesh size should be set to capture detailed geometric features [21]. The serpentine pipes were treated with local mesh encryption during meshing. Triangles were used to divide the surface mesh, and non-structural tetrahedrons were used to separate the volume mesh. The number of mesh divisions in the whole model was 1.4 million. The meshing result is shown in Figure 3.

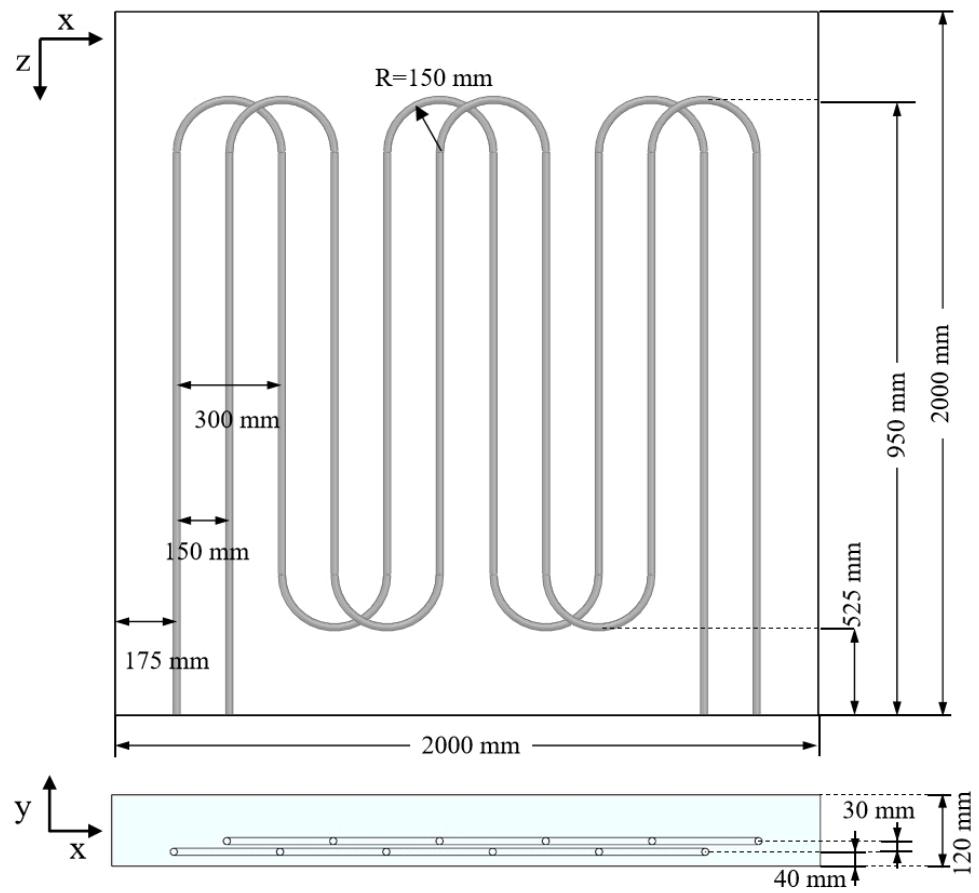


Figure 2. Dimensioning of the concrete radiant roof model.

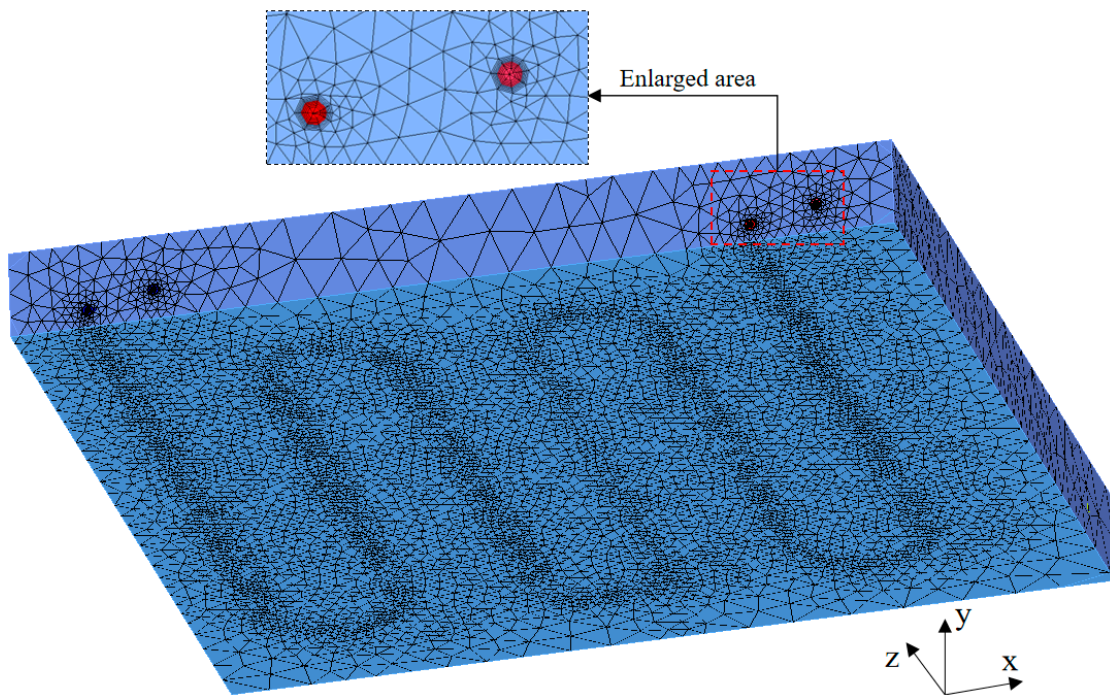


Figure 3. Grid division of the physical model.

2.3. Mathematical Model

The continuity equation is shown in Equation (1):

$$\frac{\partial \rho}{\partial t} + \frac{\partial(\rho u)}{\partial x} + \frac{\partial(\rho v)}{\partial y} + \frac{\partial(\rho w)}{\partial z} = 0 \quad (1)$$

where ρ is the fluid density, t is the time, and u , v , and w are the velocity component in x , y , and z directions, respectively.

The continuity equation is shown in Equation (2):

$$\frac{\partial(\rho \vec{U})}{\partial t} + \text{div}(\rho \vec{U} \vec{U}) = \text{div}(\mu_{eff} \text{grad} \vec{U}) \frac{\partial P}{\partial x_i} + \rho g x_i \quad (2)$$

where \vec{U} is the velocity vector of the fluid, x_i is the Cartesian coordinates, and μ_{eff} is the effective viscosity. The energy conservation equation is shown in Equation (3):

$$\frac{\partial(\rho T)}{\partial t} + \text{div}(\rho \vec{U} T) = \text{div}\left(\frac{\lambda}{c_p} \text{grad} T\right) + S_T \quad (3)$$

$$S_T = \mu_{eff} \left\{ 2 \left[\left(\frac{\partial u}{\partial x} \right)^2 + \left(\frac{\partial v}{\partial y} \right)^2 + \left(\frac{\partial w}{\partial z} \right)^2 \right] + \left(\frac{\partial u}{\partial x} + \frac{\partial v}{\partial y} + \frac{\partial w}{\partial z} \right)^2 \right\} + \lambda \text{div}(\vec{U}) \quad (4)$$

where T is the fluid temperature, λ is the heat transfer coefficient, and S_T is the source item.

For turbulent flow, μ_{eff} , in the above equation, also includes turbulent viscosity. It was necessary to add the equations in the RNG k - ε model to solve the above control equations together. The k equation and the ε equation are shown in Equations (5) and (6), respectively:

$$\frac{\partial(\rho k)}{\partial t} + \frac{\partial(\rho k U_i)}{\partial x_i} = \frac{\partial}{\partial x_i} \alpha_k \mu_{eff} \frac{\partial k}{\partial x_i} + G_k + \rho \varepsilon \quad (5)$$

$$\frac{\partial(\rho \varepsilon)}{\partial t} + \frac{\partial(\rho \varepsilon U_i)}{\partial x_i} = \frac{\partial}{\partial x_i} (\alpha_k \mu_{eff} \frac{\partial k}{\partial x_i}) + \frac{C_{1\varepsilon}^* G_k}{k} - 1.68 \frac{\varepsilon^2}{k} \quad (6)$$

$$G_k = \mu_t \left\{ 2 \left[\left(\frac{\partial u}{\partial x} \right)^2 + \left(\frac{\partial v}{\partial y} \right)^2 + \left(\frac{\partial w}{\partial z} \right)^2 \right] + \left(\frac{\partial u}{\partial x} + \frac{\partial v}{\partial y} \right)^2 + \left(\frac{\partial u}{\partial x} + \frac{\partial w}{\partial z} \right)^2 + \left(\frac{\partial v}{\partial y} + \frac{\partial w}{\partial z} \right)^2 \right\} \quad (7)$$

$$\mu_{eff} = \mu + \mu_t \quad (8)$$

$$\mu_t = 0.09 \rho \frac{k^2}{\varepsilon} \quad (9)$$

$$C_{1\varepsilon}^* = 1.42 - \frac{\eta(1 - \eta/4.377)}{1 + 0.012\eta^3} \quad (10)$$

$$\eta = \frac{\varepsilon}{k} \left(\frac{P_s}{U_i} \right)^{0.5} \quad (11)$$

where k is the turbulent kinetic energy, ε is the turbulent dissipation rate, U_i is the component of the velocity in the i direction, μ_t is the turbulent viscosity, and P_s is the turbulent shear part.

Radiation heat transfer was the focus of this paper. To obtain higher calculation accuracy, the Do radiation model with a wide range of applications was selected as the radiation model of the simulation.

2.4. Material Parameters

The simplified model included two materials: water and concrete. Two serpentine pipes of the model were set as water, and the rest was set as concrete. The thermal physical parameters of each material are shown in Table 1.

Table 1. Thermophysical parameters of materials [22].

Materials	Density kg/m ³	Thermal Conductivity W/(m ² ·K)	Specific Heat J/(kg·K)
Concrete	2500	1.74	920
Water	998.2	0.6	4182

2.5. Boundary Conditions

The boundary conditions were set according to the actual application scenario of the concrete radiant roof. The specific settings are shown in Table 2.

Table 2. Setting of boundary conditions.

Zone	Type	Name	Boundary Conditions
Water	Velocity-inlet	Inlet	Velocity Specification Method: Magnitude, Normal to Boundary
			Reference Frame: Absolute
			Velocity Magnitude: 0.3–1 m/s
	Pressure-outlet	Outlet	Temperature: 284–289 K
			Supersonic Gauge Pressure: 0 Pa
			Backflow Reference Frame: Absolute
Concrete	Wall	Wall of serpentine pipes	Gauge Pressure: 0 Pa
			Pressure Profile Multiplier: 1
			Back Direction Specification Method: Normal to Boundary
	Wall	Model top	Backflow Pressure Specification: Total Pressure
			Thermal conditions: coupled
			Thermal conditions: Heat Flux = 0 W/m ³
Wall	Model surrounding surface	Thermal conditions: Heat Flux = 0 W/m ³	
		Thermal conditions: Mixed	
		Heat Transfer Coefficient: 1.85 W/(m ² ·K)	
Wall	Model underside	Free Stream Temperature: 299 K	
		External Emissivity: 0.95	
		External Radiation Temperature: 299 K	

2.6. Solving Method

The separation solver was chosen to solve the control equation. The second-order upwind difference scheme was chosen as the discrete scheme of the control equation. The pressure difference format was the standard. The pressure–velocity coupling algorithm used the SIMPLE method. Others remained at the default settings. The convergence criterion of the energy equation was 10^{-6} . The convergence criterion of the k equation and the epsilon equation was 10^{-5} . The remaining equations converged to the standard of 10^{-3} . After the global temperature was initialized to 299 K, the flow time was set to 36,000 s to start the numerical calculation.

3. Numerical Verification

In this paper, the accuracy of the simulation method was verified by comparing the simulation results with the experimental results. The experimental results were obtained from Case 1 and Case 2 by Su et al. [23]. The simulation results were obtained by establishing and running a simulation model with the same size, boundary conditions, operating parameters, and arrangement of monitoring points as the experimental model of Su et al. [23]. The boundary conditions and operating parameters are shown in Table 3. The arrangement of monitoring points in the model is shown in Figure 4. The accuracy of the simulation model was verified by comparing the numerical simulation values and measured values of temperature monitoring points.

Table 3. Boundary conditions and operating parameters of Case1 and Case2.

Experimental Condition	Inlet Temperatures (°C)	Inlet Flow (m ³ /h)	Ambient Temperature (°C)
Case 1	12	0.3266	26.4
Case 1	13.3	0.3349	26.4

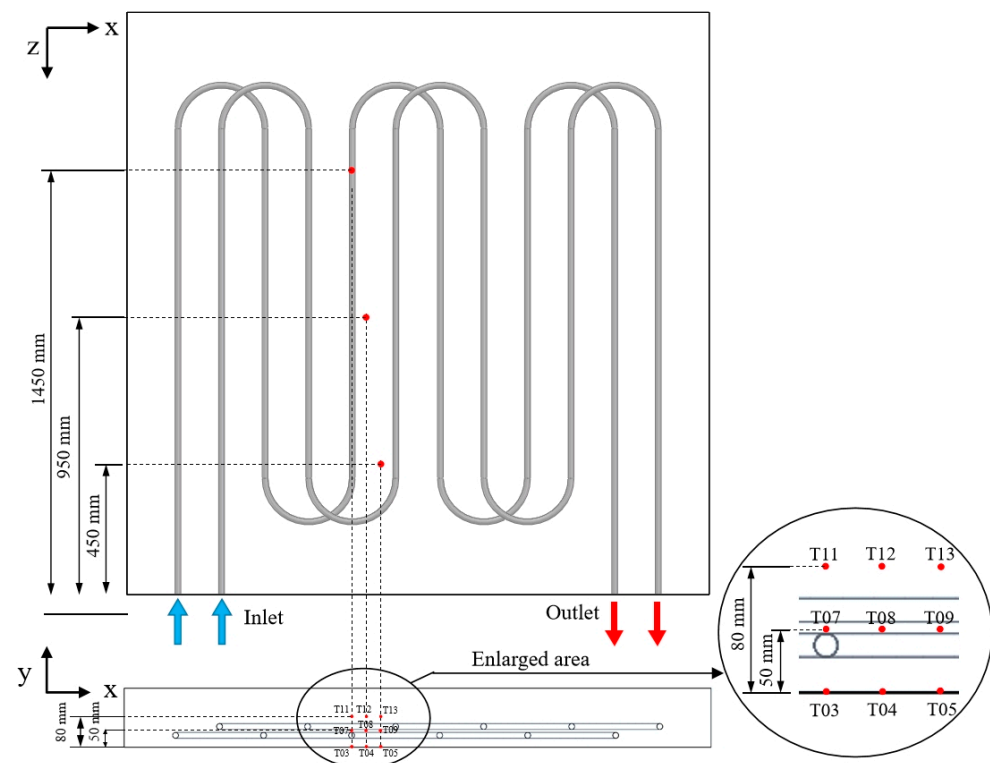


Figure 4. Arrangement of monitoring points in the model.

In Figure 5, the comparison results of Case 1 showed that the error range of monitoring points was 0.68% to 6.79%, and the average error was 4.35%. The comparison results of Case 2 showed that the monitoring points' error range was 0.54% to 6.8%, and the average error was 4.48%. The average error in both cases was less than 5%. The simulation method in this paper had good precision and can be used in the following research and discussion.

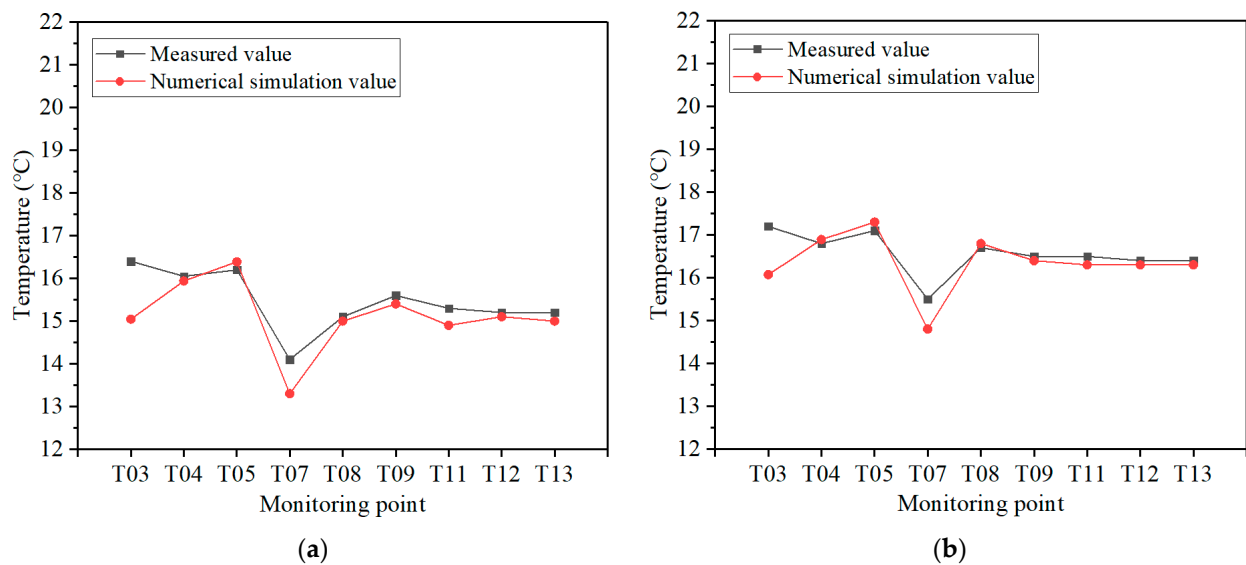


Figure 5. Comparison of simulation results and experimental results: (a) comparative results of Case 1; (b) comparative results of Case 2.

4. Results and Discussions

4.1. Heat Transfer Performance of the Concrete Radiant Roof

The purpose of this paper was to propose a reasonable anti-condensation temperature control strategy based on water supply parameter adjustment. As a result, it was necessary to study the heat transfer characteristics of the concrete radiant roof first. Three inlet velocities and six inlet temperatures were designed to analyze the radiant roof's temperature distribution and cooling capacity.

Figure 6 shows the changes in the maximum temperature, the minimum temperature, and the weighted average temperature of the radiant surface under different inlet flow velocities and temperatures. The radiant surface here refers to the bottom surface of the radiant roof in Figure 1, with the increase in the inlet temperature, the maximum temperature, the minimum temperature, and the weighted average temperature of the radiant surface all showing an increasing trend. Compared with the changes in the facet minimum temperature and the area-weighted average temperature, the change in the facet maximum temperature could have been more obvious. The increase in the inlet temperature had little influence on the maximum temperature of the radiant surface. With the increase in inlet flow velocity, the radiant surface's maximum, minimum, and weighted average temperatures all showed a slight upward trend. The inlet velocity had little effect on the temperature variation of the radiant surface.

Figure 7 shows the changes in the cooling capacity of the radiant surface under different inlet flow velocities and temperatures. With the increase in inlet velocity, the cooling capacity of the radiant surface rose slowly. With the decrease in inlet temperature, the cooling capacity of the radiant surface increased significantly. When the inlet flow velocity was 1 m/s, and the inlet temperature was 11 °C, the radiant cooling capacity reached the maximum of 71.23 W/m².

In conclusion, high inlet velocity and low inlet temperature were conducive to reducing the temperature and improving the cooling capacity of the radiant surface. However, compared with the contribution of inlet temperature, the effect of inlet flow velocity was feeble. The results were consistent with Jin et al. [11,12]. The change in water supply flow had little effect on the radiation plate temperature [11]. The change in water supply temperature was the key factor affecting the radiation plate temperature [12]. Therefore, to make the radiant roof have a good cooling capacity, we continued to conduct further investigations only on the cooling condition at the inlet temperature of 11 °C in subsequent research.

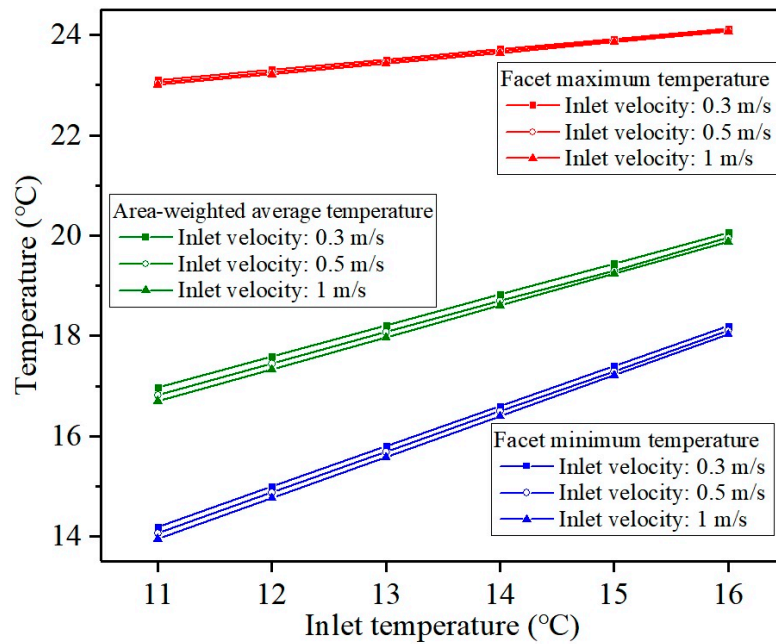


Figure 6. Temperature variation of the radiant surface.

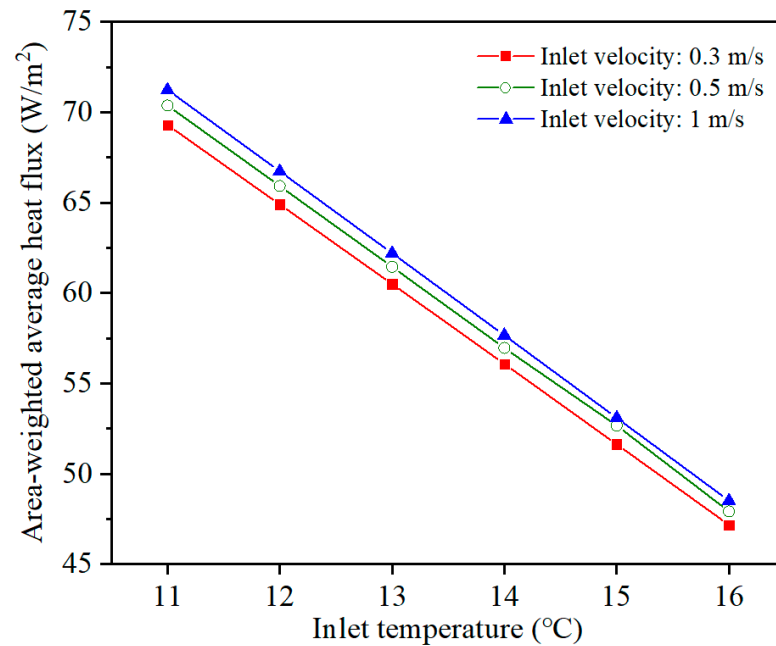


Figure 7. Cooling capacity of the radiant surface.

Figure 8 shows the temperature difference between the serpentine pipes’ outlet temperature and inlet temperature under different inlet flow velocities and temperatures. When the inlet flow rate was 0.3 m/s, the temperature difference decreased with the increase in the inlet temperature. It was found that the higher the inlet temperature, the worse the heat transfer effect between the serpentine pipes and the concrete. When the inlet velocity increased to 1 m/s, there was almost no distinction in temperature difference between the inlet temperature of 11 °C to 16 °C, and the average temperature difference was only 0.15 °C. For the inlet flow rate of 1 m/s, the temperature distribution inside the serpentine pipes was more uniform. Therefore, to make the radiant roof have a uniform and stable cooling state, we continued to conduct further research on the cooling condition at the inlet flow velocity of 1 m/s in the follow-up study.

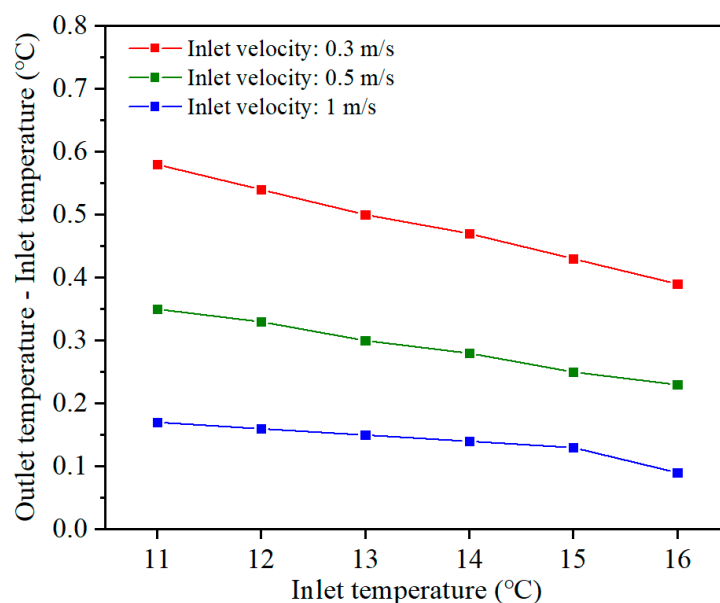


Figure 8. Change in temperature difference between outlet and inlet.

4.2. Temperature Uniformity Analysis

In order to intuitively analyze the temperature uniformity of the radiant surface, the radiant surface's temperature contour plot was shown in Figure 9 under an inlet flow velocity of 1 m/s and inlet temperature of 11 °C. The facet minimum temperature was distributed near the serpentine pipes, and the value was only 13.95 °C. The maximum facet temperature was distributed at the edge of the radiant surface, where there were no serpentine pipes, and the value reached 23.01 °C. The difference between the maximum and minimum temperature was 9.06 °C, which exceeded our expectations for the concrete radiant roof. A reasonable arrangement of the serpentine pipes will benefit a more uniform temperature distribution on the radiant surface. In addition to considering the design parameters, such as the diameter and spacing of the pipes, the distance between the serpentine pipes and the concrete's outer edge should be considered. In Figure 9, the distance between the parallel tubes of the serpentine pipes and the radiant surface's outer edge was 175 mm, and the radiant surface's outer edge temperature was about 19 °C. The distance between the bend tubes of the serpentine pipes and the radiant surface's outer edge was 300 mm, and the radiant surface's outer edge temperature was about 23 °C. Therefore, the distance between the serpentine pipes and the radiant surface's outer edge of less than 200 mm was more conducive to maintaining the temperature uniformity of the radiant surface.

4.3. Anti-Condensation Temperature Control Strategy

The root cause of condensation is that the radiant surface temperature is lower than the dew point temperature of the surrounding air. When water vapor in the air meets a radiant surface cooler than its dew point, it liquefies into water droplets and collects on the radiant surface. Once the water drops off, it will affect the user's comfort. According to the above research results, the lower the inlet temperature, the better the performance of the radiant roof. However, the lower the inlet temperature, the greater the risk of condensation. Therefore, when the minimum temperature of the radiant surface was lower than the dew point temperature, it was necessary to increase the inlet temperature to prevent condensation and improve comfort. For example, if the room temperature was 26 °C and the relative humidity was 60%, the anti-condensation temperature was 17.636 °C. Only when the inlet temperature was higher than 16 °C could the radiant surface be guaranteed without condensation. On the other hand, the water supply of 11 °C benefited from improving the heat transfer performance of the radiant roof. Thus, five temperature

control schemes were set between 11 °C and 16 °C of the inlet temperature, as shown in Table 4.

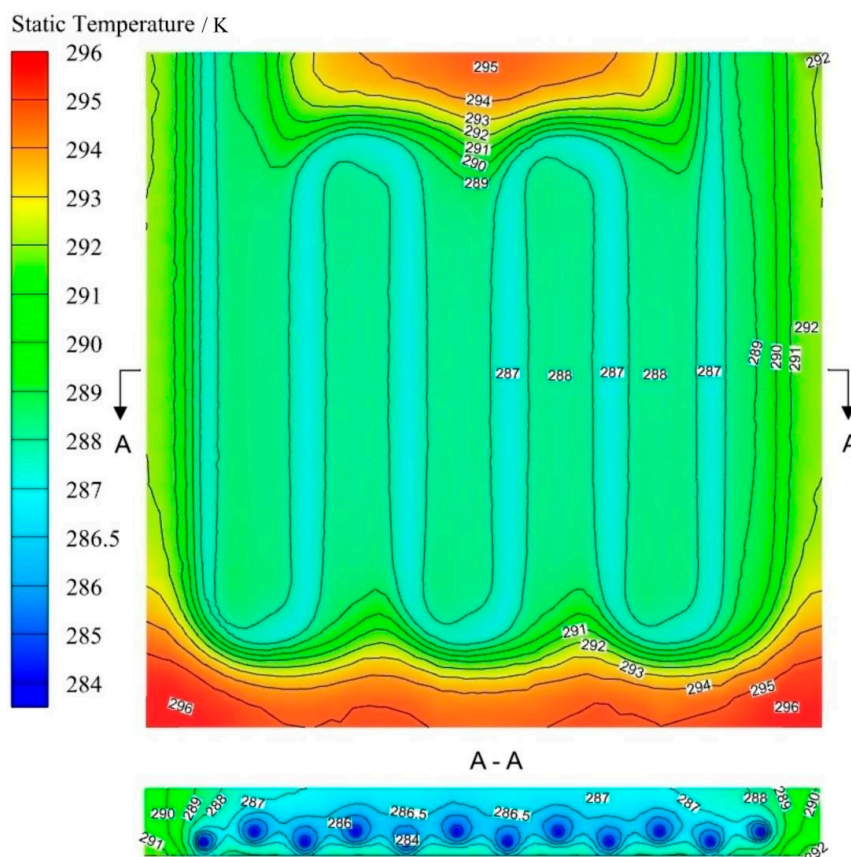


Figure 9. Radiant surface’s temperature contour plot.

Table 4. Temperature control strategy of five schemes.

Time	Inlet Temperature					
	11 °C	12 °C	13 °C	14 °C	15 °C	16 °C
Scheme 1	1705 s	1000 s	/	/	/	/
Scheme 2	1705 s	/	1000 s	/	/	/
Scheme 3	1705 s	/	/	2895 s	9330 s	22,070 s
Scheme 4	1705 s	/	/	/	14,300 s	19,995 s
Scheme 5	1705 s	/	/	/	/	34,295 s

As shown in Figure 10 and Table 4, the inlet temperature of the five schemes at the beginning stage was 11 °C. When the minimum temperature of the radiant surface reached the dew point temperature of 17.636 °C, the inlet temperature was switched to 12 °C (Scheme 1), 13 °C (Scheme 2), 14 °C (Scheme 3), 15 °C (Scheme 4), and 16 °C (Scheme 5), respectively. For Scheme 1 and Scheme 2, when the inlet temperature was switched from 11 °C to 12 °C and 13 °C, the minimum temperature remained below 17.636 °C and continued to drop. Currently, Schemes 1 and 2 did not eliminate the condensation phenomenon, so it was not recommended to continue the research. For Schemes 3, 4, and 5, when the inlet temperature was switched from 11 °C to 14 °C, 15 °C, and 16 °C, the minimum temperature was below 17.636 °C for a short time and then higher than 17.636 °C shortly thereafter. Schemes 3, 4, and 5 effectively prevent condensation. According to the research in Section 4.1, for Schemes 3 and 4, when the inlet temperature remained unchanged at 14 °C and 15 °C, there was still a condensation risk when the minimum temperature was lower than 17.636 °C and it was still necessary to adjust the inlet temperature rise.

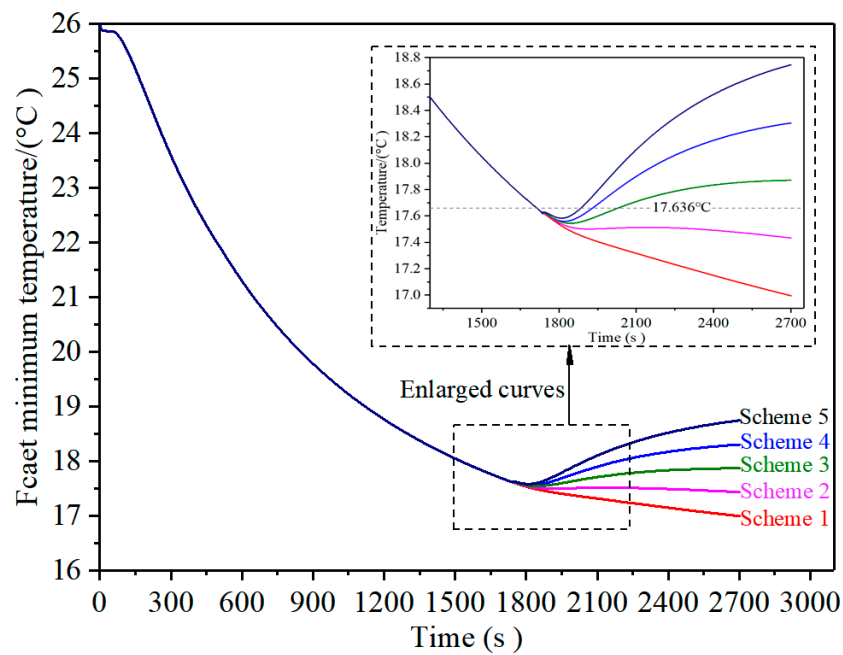


Figure 10. Anti-condensation control results within 3000 s.

Figure 11 shows the anti-condensation result of the radiant roof during the whole cooling process until it was stable under Schemes 3, 4, and 5. The facet minimum temperature under the three schemes was higher than 17.636 °C. No condensation appeared in the radiant roof during the cooling and stabilizing process. Near the several minimum values on each facet minimum temperature curve, the inlet temperature was increased to avoid a further reduction in the temperature value under the previous inlet temperature. It was apparent that a moderate increase in inlet temperature could effectively avoid the condensation of the radiant surface. From the above analysis, it could be seen that, for the radiant roof whose inlet temperature was 11 °C, when the facet minimum temperature was close to the dew point temperature, it was necessary to ensure that the inlet temperature rose by at least 3 °C to create an inflection point of temperature rise and thus decrease condensation. For the radiant roof with an inlet temperature above 14 °C, when the facet minimum temperature was close to the dew point temperature, the inlet temperature could be increased by 1 °C to slow down condensation. The cooling capacity of the radiant roof was gradually increased throughout the cooling process. It was worth noting that the heat flux had a different increase when the inlet temperature changed. When the inlet temperature was lower, the heat flux increased more obviously. In order to obtain higher refrigeration capacity, the inlet temperature of the radiant roof is controlled at a low value as much as possible while ensuring anti-condensation. Among the three schemes, Scheme 3 was the most consistent with this design principle. During the whole cooling process, the cooling temperature at any time was lower than that of the other two schemes, and the heat flux was also the highest at any time. Therefore, Scheme 3 was our preferred option. The principle of this control strategy was to increase the operating time of the lower inlet temperature as much as possible. The temperature control strategy for the cooling process of the radiant panel was as follows: set the inlet temperature to 11 °C, the first anti-condensation control inlet temperature to 14 °C, the second anti-condensation control inlet temperature to 15 °C, and the third anti-condensation control inlet temperature to 16 °C until stable operation. The temperature control strategy not only prevented condensation but also improved the cooling performance of the radiant roof. However, the above scheme could only improve the thermal performance of the radiant roof in the cooling process. Due to the restriction of condensation, the inlet temperature in the final stability stage was greatly limited.

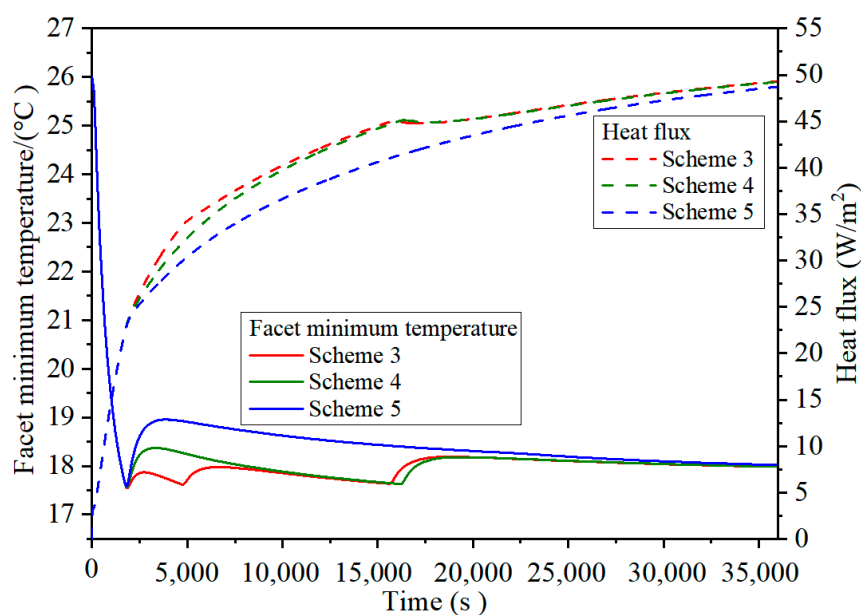


Figure 11. Anti-condensation control results within 36,000 s.

5. Conclusions

This paper used a computational fluent dynamics (CFD) simulation with Ansys Fluent to establish a concrete radiant roof model. After verifying the model's accuracy, we studied the concrete radiant roof model's heat transfer performance, temperature uniformity analysis, and anti-condensation temperature control strategy. The conclusions were as follows:

1. In terms of the accuracy of the research, the simulation error was less than 5% compared with the experimental results of Su et al. [23];
2. In thermal performance research, the cooling capacity increased with the increase in inlet flow rate and the decrease in temperature. Compared with the inlet flow rate, the inlet temperature significantly impacted the cooling capacity and radiant surface temperature, which could be used as the primary adjustment parameter of the subsequent anti-condensation temperature control strategy;
3. In the uniformity study, the temperature uniformity of the concrete radiant roof was not ideal, and the difference between the maximum and minimum temperatures was as high as 9.06 °C. The distance between the serpentine pipes area and the concrete edge became the fundamental reason that affected the temperature uniformity. The distance between the serpentine pipes and the radiant surface's outer edge of less than 200 mm was more conducive to maintaining the temperature uniformity of the radiant surface;
4. Regarding anti-condensation and performance improvement research, first supplying water at low temperatures and then dynamically adjusting high-temperature water could effectively avoid condensation and improve the radiant roof's heat transfer performance. Nevertheless, the performance improvement was limited to the cooling process. For the long-term stable operation of the radiation roof, the inlet temperature was usually stable and unchanged, maintained at a high value. The water supply temperature, when the radiant roof was finally stabilized, was still limited by the dew point temperature.

Author Contributions: Conceptualization, B.Z., Q.S. and K.D.; methodology, B.Z. and K.D.; software, W.W.; validation, B.Z., L.S. and W.W.; formal analysis, H.G.; investigation, W.L.; data curation, Z.S.; writing—original draft preparation, B.Z. and Q.S.; writing—review and editing, B.Z., Q.S. and K.D.; project administration, K.D. All authors have read and agreed to the published version of the manuscript.

Funding: This research was funded by the Guangdong Basic and Applied Basic Research Foundation [grant number 2019A1515111177], the Guangzhou Science and Technology Plan Project [grant number 202201010108], and the Guangzhou Development Zone International Science and Technology Cooperation Project Funding [grant number 2021GH07].

Conflicts of Interest: The authors declare no conflict of interest.

References

1. Rhee, K.N.; Kim, K.W. A 50 year review of basic and applied research in radiant heating and cooling systems for the built environment. *Build. Environ.* **2015**, *91*, 166–190. [[CrossRef](#)]
2. Tian, Z.; Love, J.A. A field study of occupant thermal comfort and thermal environments with radiant slab cooling. *Build. Environ.* **2008**, *43*, 1658–1670. [[CrossRef](#)]
3. Rhee, K.N.; Olesen, B.W.; Kim, K.W. Ten questions about radiant heating and cooling systems. *Build. Environ.* **2017**, *112*, 367–381. [[CrossRef](#)]
4. Karmann, C.; Schiavon, S.; Bauman, F. Thermal comfort in buildings using radiant vs. all-air systems: A critical literature review. *Build. Environ.* **2016**, *111*, 123–131. [[CrossRef](#)]
5. Olesen, B.W.; De Carli, M.; Scarpa, M.; Koschenez, M. Dynamic evaluation of the cooling capacity of thermal active building systems. *ASHRAE Trans.* **2006**, *112*, 350–357.
6. Hu, R.; Niu, J. A review of the application of radiant cooling and heating systems in Mainland China. *Energy Build.* **2012**, *52*, 11–19. [[CrossRef](#)]
7. Psomas, T.; Teli, D.; Langer, S.; Wahlgren, P.; Wargocki, P. Indoor humidity of dwellings and association with building characteristics, behaviors and health in a northern climate. *Build. Environ.* **2021**, *1*, 107885. [[CrossRef](#)]
8. Memon, R.A.; Chirarattananon, S.; Vangtook, P. Thermal comfort assessment and application of radiant cooling. *Build. Environ.* **2008**, *43*, 1185–1196. [[CrossRef](#)]
9. Zhang, L.Z. Energy performance of independent air dehumidification systems with energy recovery measures. *Energy* **2006**, *31*, 1228–1242. [[CrossRef](#)]
10. Ziarani, N.N.; Haghighi, A.P. Anticipating an efficient relative humidity in a room under direct solar radiation and equipped by radiant cooling panel system. *Int. J. Refrig.* **2019**, *98*, 98–108. [[CrossRef](#)]
11. Jin, W.; Jiang, J.; Jia, L.; Wang, Z. The dynamic effect of supply water flow regulation on surface temperature changes of radiant ceiling panel for cooling operation. *Sustain. Cities Soc.* **2019**, *52*, 101765. [[CrossRef](#)]
12. Jin, W.; Ma, J.; Jia, L.; Wang, Z. Dynamic Variation of Surface Temperatures on the Radiant Ceiling Cooling Panel based on the Different Supply Water Temperature Adjustments. *Sustain. Cities Soc.* **2019**, *52*, 101805. [[CrossRef](#)]
13. Wongkee, S.; Chirarattananon, S.; Chaiwiwatworakul, P. A field study of experimental of radiant cooling for residential building in a tropical climate. *J. Autom. Control. Eng.* **2014**, *2*, 67–70. [[CrossRef](#)]
14. Conroy, C.L.; Mumma, S.A. Ceiling radiant cooling panels as a viable distributed parallel sensible cooling technology integrated with DOAS. *ASHRAE Trans.* **2001**, *107*, 578–588.
15. Kang, Z.; Peng, X.; Cheng, X.; Feng, G. Analysis of condensation and thermal comfort of two kinds of compound radiant cooling air conditioning systems based on displacement ventilation. *Procedia Eng.* **2017**, *205*, 1529–1534. [[CrossRef](#)]
16. Hout, M.; Ghaddar, N.; Ghali, K.; Ismail, N.; Simonetti, M.; Fracastoro, G.V.; Virgone, J.; Zoughaib, A. Displacement ventilation with cooled liquid desiccant dehumidification membrane at ceiling; modeling and design charts. *Energy* **2017**, *139*, 1003–1015. [[CrossRef](#)]
17. Chun, L.; Gong, G.; Fang, X.; Peng, P. Thermodynamic performance assessment of vacuum membrane-based dehumidification and air carrying energy radiant airconditioning system (vmd-acers). *Chin. J. Chem. Eng.* **2021**, *34*, 217–227. [[CrossRef](#)]
18. Tang, H.; Liu, X.H.; Li, H.; Zhou, Y.; Jiang, Y. Study on the reduction of condensation risks on the radiant cooling ceiling with superhydrophobic treatment. *Build. Environ.* **2016**, *100*, 135–144. [[CrossRef](#)]
19. Ning, B.; Chen, Y.; Liu, H.; Zhang, S. Cooling capacity improvement for a radiant ceiling panel with uniform surface temperature distribution. *Build. Environ.* **2016**, *102*, 64–72. [[CrossRef](#)]
20. Kong, X.; Zhang, D.; Zhang, X. Design and analysis of “leading condensation” radiant panel. *J. Jiangsu Univ. Sci. Technol. Nat. Sci. Ed.* **2011**, *25*, 440–442.
21. Gao, J.; Zhang, D.; Yang, M. The influence of mesh generation on the results of flow solving in working face and gob. *Procedia Eng.* **2013**, *37*, 125–131. [[CrossRef](#)]
22. Lu, Y. *Heating and Ventilation Design Manual*, 1st ed.; China Building Industry Press: Beijing, China, 1987; pp. 96–120.
23. Su, L.; Li, N.; Zhang, X. Experimental Study on Cooling Characteristics of Concrete Ceiling Radiant Cooling Panel. *Procedia Eng.* **2015**, *121*, 2168–2175. [[CrossRef](#)]

Disclaimer/Publisher’s Note: The statements, opinions and data contained in all publications are solely those of the individual author(s) and contributor(s) and not of MDPI and/or the editor(s). MDPI and/or the editor(s) disclaim responsibility for any injury to people or property resulting from any ideas, methods, instructions or products referred to in the content.